Materials Horizons

ROYAL SOCIETY OF CHEMISTRY

COMMUNICATION

View Article Online
View Journal | View Issue

Published on 13 August 2024. Downloaded by Institute of Physics, CAS on 10/29/2024 4:28:02 AM.

Check for updates

Cite this: *Mater. Horiz.*, 2024, **11**, 5394

Received 21st June 2024,
Accepted 9th August 2024

DOI: 10.1039/d4mh00795f

rsc.li/materials-horizons

Mixed anion control of enhanced negative thermal expansion in the oxysulfide of $PbTiO_3$†

Zhao Pan, *[ab] Zhengli Liang, [c] Xiao Wang, [a] Yue-Wen Fang, *[de] Xubin Ye,[a] Zhehong Liu,[a] Takumi Nishikubo,[fb] Yuki Sakai,[fb] Xi Shen,[a] Qiumin Liu,[b] Shogo Kawaguchi, [g] Fei Zhan,[h] Longlong Fan,[h] Yong-Yang Wang,[h] Chen-Yan Ma,[h] Xingxing Jiang,[c] Zheshuai Lin, [c] Richeng Yu, [a] Xianran Xing, *[i] Masaki Azuma [bf] and Youwen Long *[aj]

The rare physical property of negative thermal expansion (NTE) is intriguing because materials with a large NTE over a wide temperature range can serve as high-performance thermal expansion compensators. However, the applications of NTE are hindered by the fact that most of the available NTE materials show small magnitudes of NTE, and/or NTE occurs only in a narrow temperature range. Herein, for the first time, we investigated the effect of anion substitution instead of general Pb/Ti-site substitutions on the thermal expansion properties of a typical ferroelectric NTE material, $PbTiO_3$. Intriguingly, the substitution of S for O in $PbTiO_3$ further increases the tetragonality of $PbTiO_3$. Consequently, an unusually enhanced NTE with an average volumetric coefficient of thermal expansion of $\bar{\alpha}_V = -2.50 \times 10^{-5}$ K^{-1} was achieved over a wide temperature range (300–790 K), which is in contrast to that of pristine $PbTiO_3$ ($\bar{\alpha}_V = -1.99 \times 10^{-5}$ K^{-1}, RT–763 K). The intensified NTE is attributed to the enhanced hybridization between Pb/Ti and O/S atoms by the substitution of S, as evidenced by our theoretical investigations. We therefore demonstrate a new technique for introducing mixed anions to achieve a large NTE over a wide temperature range in $PbTiO_3$-based ferroelectrics.

New concepts

$PbTiO_3$ (PT) is a typical perovskite-type (ABO_3) ferroelectric, which also exhibits unique negative thermal expansion (NTE) properties. Materials with a strong NTE are very important, since they can be used to tailor the overall coefficient of thermal expansion (CTE) of materials, or even realize the favorable zero thermal expansion. While much attention has been paid to modifying the NTE properties of PT by replacing A-site Pb and/or B-site Ti cations, the effect of anion-site substitution on the NTE of PT remains unknown. Therefore, a feasible mixed anion control of the thermal expansion of PT was proposed. An unusually enhanced NTE over a wide temperature range was achieved in the oxysulfide of $PbTiO_3$, which was evidenced by comprehensive experimental and theoretical studies. The anion-mediated enhanced NTE demonstrates a new technique for realizing a large NTE in PT-based perovskites, providing a new way for the design of high-performance NTE functional materials.

1. Introduction

Controlling thermal expansion is an important topic in fundamental research and a critical issue in practical applications, particularly in high-precision applications subject to large temperature fluctuations, such as electronic devices and optical instruments.[1–5] The discovery of negative thermal expansion (NTE) materials, in which the volume shrinks instead of expansion upon heating in a certain temperature range, offers a

[a] *Beijing National Laboratory for Condensed Matter Physics, Institute of Physics, Chinese Academy of Sciences, Beijing 100190, China. E-mail: zhaopan@iphy.ac.cn, ywlong@iphy.ac.cn*
[b] *Laboratory for Materials and Structures, Tokyo Institute of Technology, 4259 Nagatsuta, Midori, Yokohama, 226-8503, Japan*
[c] *Center for Crystal R&D, Key Laboratory of Functional Crystals and Laser Technology, Technical Institute of Physics and Chemistry, Chinese Academy of Sciences, Beijing 100190, China*
[d] *Fisika Aplikatua Saila, Gipuzkoako Ingeniaritza Eskola, University of the Basque Country (UPV/EHU), Europa Plaza 1, 20018 Donostia/San Sebastián, Spain. E-mail: yuewen.fang@ehu.eusmailto, fyuewen@gmail.com*
[e] *Centro de Física de Materiales (CSIC-UPV/EHU), Manuel de Lardizabal Pasealekua 5, 20018 Donostia/San Sebastián, Spain*
[f] *Kanagawa Institute of Industrial Science and Technology (KISTEC), 705-1 Shimoimaizumi, Ebina, Kanagawa 243-0435, Japan*
[g] *Research and Utilization Division, Japan Synchrotron Radiation Research Institute (JASRI), SPring-8, 1-1-1 Kouto, Sayo-cho, Sayo-gun, Hyogo 679-5198, Japan*
[h] *Synchrotron Radiation Laboratory, Institute of High Energy Physics, Chinese Academy of Sciences, Beijing 100049, China*
[i] *Beijing Advanced Innovation Center for Materials Genome Engineering and Department of Physical Chemistry, University of Science and Technology Beijing, Beijing 100083, China. E-mail: xing@ustb.edu.cn*
[j] *Songshan Lake Materials Laboratory, Dongguan, Guangdong 523808, China*

† Electronic supplementary information (ESI) available. See DOI: https://doi.org/10.1039/d4mh00795f

This journal is © The Royal Society of Chemistry 2024

Published on 13 August 2024. Downloaded by Institute of Physics, CAS on 10/29/2024 4:28:02 AM.

promising opportunity to tailor the coefficient of thermal expansion (CTE) of the materials. Such materials can be combined with normal positive thermal expansion (PTE) materials to form composites with controllable positive, negative, or even zero thermal expansion (ZTE). In the past decades, a wide variety of materials have been reported to exhibit NTE, including oxides,[6–14] alloys,[15–20] nitrides,[21–23] fluorides,[24–28] cyanides,[29–31] and reduced ruthenates.[32–34] Although the control of thermal expansion is important, such behavior can be difficult to achieve. Indeed, most of the present NTE materials show small magnitudes of NTE, and NTE usually occurs in a narrow temperature range, which limits the applications of such NTE materials. Therefore, achieving a large NTE over a wide temperature range remains a great challenge.

Among the currently available NTE materials, $PbTiO_3$ (PT)-based ferroelectric NTE materials are particularly interesting. PT is a typical perovskite-type (ABO_3) ferroelectric with a large tetragonality (c/a) of 1.064.[35] In addition to ferroelectricity, PT exhibits a unique NTE in the perovskite family.[7] The unit cell volume of PT contracts over a wide temperature range from room temperature to its Curie temperature (T_C = 763 K) in the tetragonal ferroelectric phase, with an average intrinsic bulk CTE of $\bar{\alpha}_V = -1.99 \times 10^{-5}$ K^{-1}.[36] Owing to the advantage of a flexible perovskite structure, the NTE properties of PT can be efficiently controlled by varying the substitutions at the A-site Pb and B-site Ti atoms.[3] Because the volume shrinkage of PT only occurs along the polar c axis of the tetragonal phase, it is proposed that the increase in c/a could induce a larger NTE. Indeed, enhanced NTE was obtained in PT-based ferroelectrics with improved tetragonality.[37–40] Nevertheless, most substitutions in PT result in reduced tetragonality and weakened NTE (see panel I in Fig. 1), and only a few PT-based ferroelectrics exhibit unusually improved tetragonality and enhanced NTE compared with pristine PT (see panel II in Fig. 1).

To date, all modifications of the NTE properties of PT have focused on A- and/or B-site cation substitutions, while no studies have reported on the effect of substitutions at the anion O site on the NTE of PT. One possible reason for this could be the difficulty in preparing PT-based mixed-anion compounds. However, the differences in the valences, electronegativities, and ionic radii of heteroanions are expected to affect the crystal and electronic structures of PT and, therefore, modify the NTE behavior.[41] In the present study, we successfully synthesized the oxysulfide of $PbTiO_3$ using a unique high-pressure and high-temperature (HPHT) method. Intriguingly, improved tetragonality accompanied by an unusually enhanced NTE was obtained, which indicates that the introduction of anions could be a new and effective way to achieve a large NTE in PT-based ferroelectric NTE materials.

2. Results and discussion

According to the X-ray diffraction (XRD) patterns of the $PbTiO_{3-x}S_x$ compounds (Fig. 2(b)), all the samples are of high quality with a perovskite structure (Fig. 2(a)). Note that impurities appeared for x values higher than 0.02, indicating the solid solubility limit was reached under those synthesis conditions. Although the substitution content of sulfur was low, the S distribution was very uniform in the lattice according to the elemental distribution

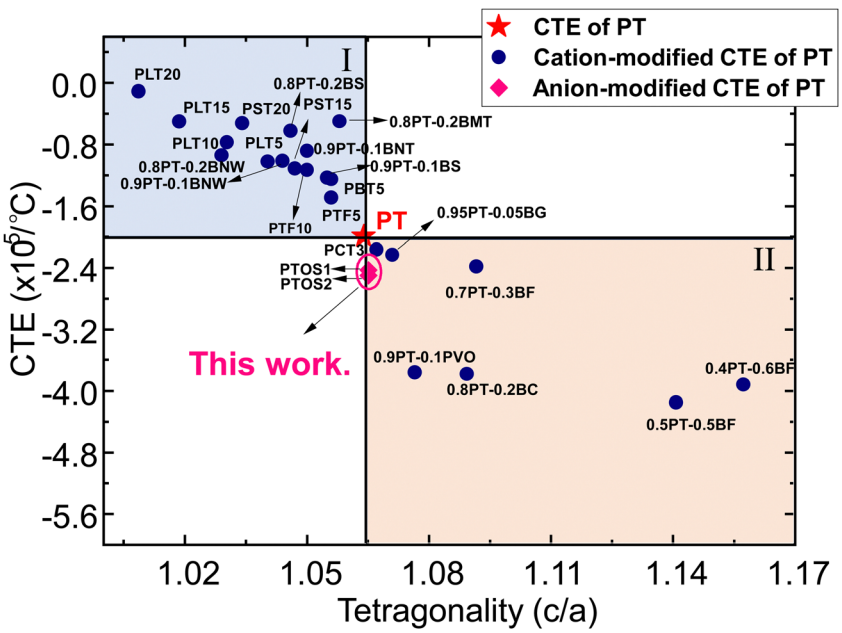

Fig. 1 Relationship between tetragonality (c/a) and the coefficient of thermal expansion (CTE) in PT-based ferroelectrics. Herein, PLT100x is the abbreviation of $Pb_{1-x}La_xTiO_3$, PST100x indicates $Pb_{1-x}Sr_xTiO_3$, PTF100x stands for $Pb(Ti_{1-x}Fe_x)O_3$, PBT100x represents $(Pb_{1-x}Bi_x)TiO_3$, $(1-x)$PT–xBNT indicates $(1-x)PbTiO_3$–$xBi(Ni_{1/2}Ti_{1/2})O_3$, PCT100x stands for $Pb_{1-x}Cd_xTiO_3$, $(1-x)$PT–xPV represents $(1-x)PbTiO_3$–$xPbVO_3$, $(1-x)$PT–xBF indicates $(1-x)PbTiO_3$–$xBiFeO_3$, and $(1-x)$PT–xBC indicates $(1-x)PbTiO_3$–$xBiCoO_3$.[3]

Published on 13 August 2024. Downloaded by Institute of Physics, CAS on 10/29/2024 4:28:02 AM.

analysis (Fig. S1, ESI†). Additionally, according to the XANES spectra, the main absorption at the S-K edge of PTOS2 is located at 2472.8 eV (Fig. S2, ESI†), which is identical to the results reported for S^{2-},[42] thus suggesting the existence of S^{2-} in the PTOS compounds. In addition, the calculated structure is almost consistent with the XANES experimental data (Fig. S2(b), ESI†). The shoulder in the calculated structure at around 2474 eV could be attributed to the effect of the Pb M_5 edge (2484 eV), which is near the S K edge. Note that all the investigated samples can be indexed to the tetragonal symmetry with the space group of *P4mm*. The detailed structural parameters for the $PbTiO_{3-x}S_x$ compounds were refined using synchrotron X-ray diffraction (SXRD) data and are presented in Fig. S3, S4 and Table S1 (ESI†). With the substitution of S for O, there is almost no shift of the (001) peak, indicating the *c* axis is stable. However, the (100) peak exhibits an apparent shift toward the higher angle region as a function of S (see the amplified part around $2\theta \approx 21$–23° in Fig. 2(b)), which suggests the contraction of the *a* axis. As a result, the *c*/*a* ratio slightly increased from 1.064 for pristine PT to ~1.065 for PTOS1 and PTOS2 (Fig. 2(c)), which implies the enhanced tetragonality by substitution of S. The enhanced tetragonality can be attributed to the strong Pb–O/S and Ti–O/S hybridizations, which will be discussed in detail later.

Based on the lattice dynamic theory, the vibrational soft modes are proposed to be closely related to the ferroelectric phase transition. It is suggested that the frequency of the A_1(1TO) soft mode is proportional to the order parameter of spontaneous polarization (P_S) as it represents the displacement of the BO_6 octahedron relative to A-site atoms in perovskite-type ferroelectric materials. Therefore, the A_1(1TO) soft mode can indicate the variation of P_S in PT-based perovskites with both normally reduced *c*/*a* and abnormally enhanced *c*/*a*. For example, an enhanced *c*/*a* accompanied by hardened A_1(1TO) was observed in $Pb_{1-x}Cd_xTiO_3$,[37] whereas an opposite tendency of reduced *c*/*a* and softened A_1(1TO) was observed in $Pb_{1-x}Sr_xTiO_3$.[43] The Raman spectra of the present PTOS compounds are shown in Fig. 2(d). Intriguingly, the Raman active modes of A_1(1TO) abnormally show a slight shift to higher frequencies with increasing S content, which is consistent with the enhanced *c*/*a*. Note that this is the first observation of mixed anion control of enhanced tetragonality in $PbTiO_3$-based perovskites.

As mentioned before, in PT-based ferroelectric NTE materials, the enhanced *c*/*a* could be related to a large ferroelectric volume effect, that is, a large NTE.[40,44] Generally, a large *c*/*a* of PT-based ferroelectrics indicates a large lattice distortion and can result in a large volume shrinkage. Consequently, a large NTE can usually be obtained in PT-based systems with an enhanced *c*/*a* compared to that of pristine PT.[3] To study the thermal expansion properties of the present PTOS100*x* compounds with increased tetragonality, the temperature-dependent SXRD experiment was performed for the PTOS1 and PTOS2 samples. The unit cell volume as a function of temperature was extracted by structural refinement based on SXRD data. Pristine PT exhibits a nonlinear and strong NTE from RT to 800 K with an average volumetric CTE

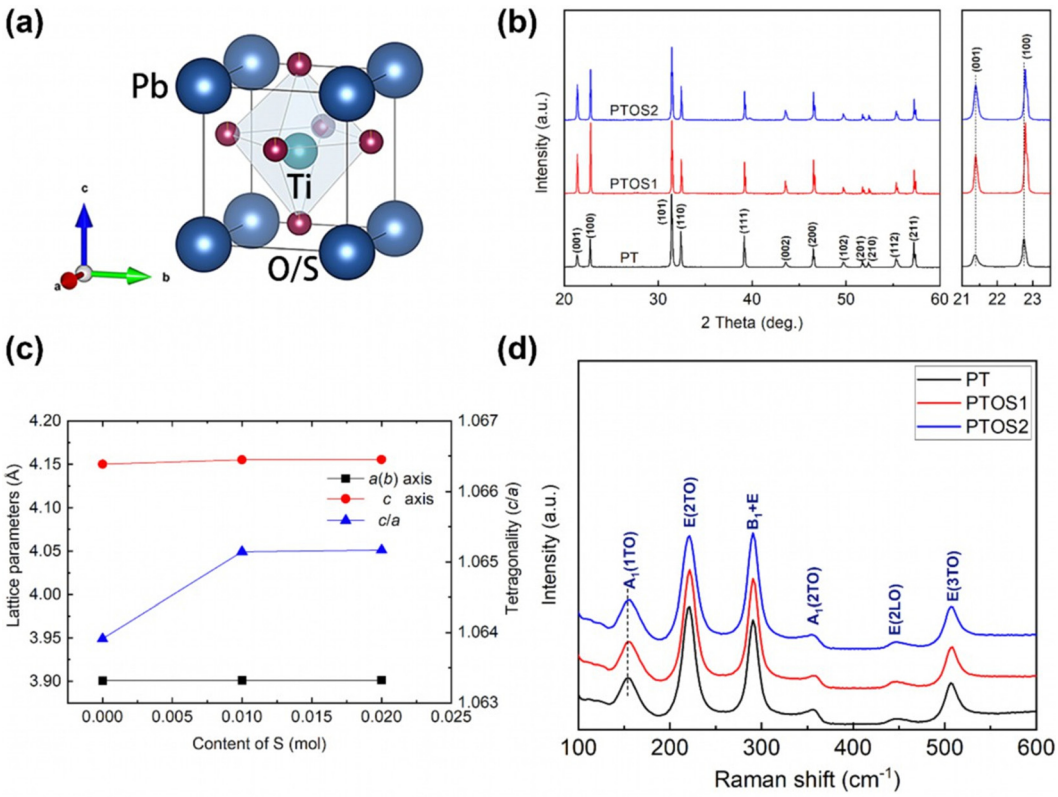

Fig. 2 Crystal structure and lattice parameters of $PbTiO_{3-x}S_x$. (a) Schematic of the perovskite structure with a *P4mm* symmetry. (b) Evolution of XRD patterns, (c) tetragonality (*c*/*a*) (the error bars are much smaller than the symbols), and (d) Raman spectra of the $PbTiO_{3-x}S_x$ (x = 0, 0.01, and 0.02) compounds as a function of sulfide concentration at room temperature.

 This journal is © The Royal Society of Chemistry 2024

Published on 13 August 2024. Downloaded by Institute of Physics, CAS on 10/29/2024 4:28:02 AM.

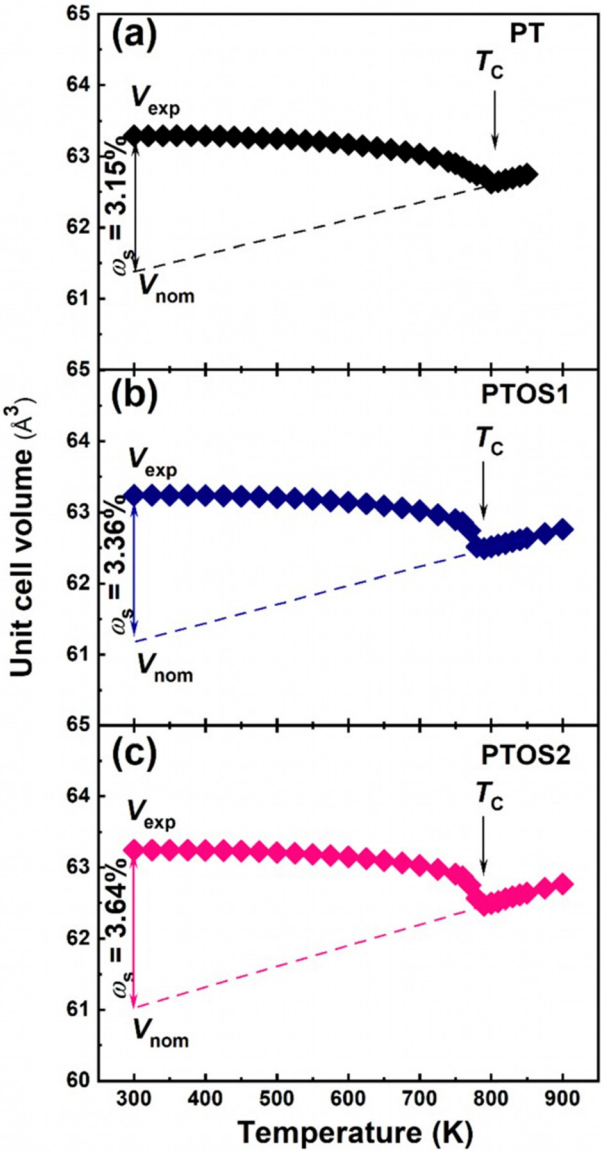

Fig. 3 Thermal expansion properties. Temperature dependence of the unit cell volume of the $PbTiO_{3-x}S_x$ compounds: (a) x = 0, (b) x = 0.01, and (c) x = 0.02. The schematic diagram of spontaneous volume ferroelectrostriction (ω_S) and T_C is also presented. Note that the error bars are much smaller than the symbols.

of $\bar{\alpha}_V = -2.11 \times 10^{-5}$ K^{-1} (Fig. 3(a)). Notably, the difference in the CTE of PT between the present study and the previous report could be attributed to the different accuracy of sample temperatures during the high-temperature XRD measurements. With the substitution of S for O, the PTOS1 compound exhibits a nonlinear but stronger NTE from room temperature (RT) to $T_C \approx 790$ K with an average volumetric CTE of $\bar{\alpha}_V = -2.43 \times 10^{-5}$ K^{-1} (Fig. 3(b)). With a further increase in the content of S for the PTOS2 compound relative to PTOS1, the magnitude of NTE continued to increase, and a further enhanced NTE with an average volumetric CTE of $\bar{\alpha}_V = -2.50 \times 10^{-5}$ K^{-1} was achieved over a wide temperature range from RT to 790 K (Fig. 3(c)) for PTOS2. Herein, we successfully achieved an enhanced NTE of PT by anion substitution for the first time, which provides a new strategy for obtaining a large NTE in PT-based ferroelectric NTE materials.

In comparison, the NTE in the present PTOS is much stronger than those in many PT-based ferroelectrics, with enhanced NTE compared to the pristine PT, such as $Pb_{0.97}Cd_{0.03}TiO_3$ (c/a = 1.066, $\bar{\alpha}_V = -2.16 \times 10^{-5}$ K^{-1}, 300–743 K)[37] and 0.95PT–0.05$BiGaO_3$ (c/a = 1.071, $\bar{\alpha}_V = -2.23 \times 10^{-5}$ K^{-1}, 300–773 K).[38] Additionally, the present NTE is even comparable to typical framework NTE materials, such as ZrW_2O_8 ($\bar{\alpha}_V = -2.73 \times 10^{-5}$ K^{-1}, 0.3–1050 K) and $Fe[Co(CN)_6]$ ($\bar{\alpha}_V = -4.41 \times 10^{-6}$ K^{-1}, 4.2–300 K),[6,29] which were usually reported to show strong NTE.

According to vast experimental and theoretical studies of PT-based ferroelectric NTE materials, ferroelectric behavior plays an important role in the NTE of PT-based ferroelectrics.[3,45] A new physical concept of spontaneous volume ferroelectrostriction (SVFS, ω_S) was recently proposed to quantitatively elucidate the effect of ferroelectricity on the anomalous volume change in the tetragonal ferroelectric phase of PT-based ferroelectrics, where the baseline of the description of SVFS can be estimated for the contribution purely by the thermal expansion of phonon vibration.[46] The SVFS effect can be defined by the following equation:

$$\omega_S = \frac{V_{exp} - V_{nm}}{V_{nm}} 100\%$$

where V_{exp} and V_{nm} indicate the experimental and nominal unit cell volumes, respectively. Here, V_{nm} can be estimated by extrapolation from the paraelectric phase to the ferroelectric phase. Note that a large value of ω_S indicates a strong ferroelectrovolume effect and an enhanced NTE, whereas a small value indicates a weak NTE. The ω_S values were 3.36% and 3.64% for the PTOS1 and PTOS2 compounds (Fig. 3), respectively, which are much higher than that of PT (3.1%).[3] The above results are consistent with the enhanced NTE observed in PTOS1 and PTOS2.

According to the previous studies,[47,48] the hybridization between the cations and anions is crucial to the NET in PT-based ferroelectrics. To understand the hybridization, we have used first-principles calculations to understand the effect of sulfur doping on lead titanate. Because the concentration in the actual $PbTiO_{3-x}S_x$ samples is relatively small (x = 0.01 and 0.02), it is not practical in standard density functional theory (DFT) calculations using the supercell method. To implement the modeling, we substitute one (two) sulfur atom(s) for one (two) oxygen atom(s) to approximate PTOS1 and PTOS2 in a 2 × 2 × 2 40-atom supercell. In pristine $PbTiO_3$, there are two different Wyckoff sites 1b and 2c. To find the lowest-energy doped structure, we performed total energy calculations for all the possible structure configurations of PTOS1 and PTOS2. The energetic profile is shown in Fig. 4(a). We find that both PTOS1 and PTOS2 prefer the S doping at the 1b site energetically. To simplify the analysis, we just studied the properties of the two lowest energy states of PTOS1 and PTOS2. Because all the studied structures have a tetragonal crystal system, there are six independent elastic constants determined by the symmetry.[49] Based on Born–Huang conditions,[50] the following inequality criteria

Published on 13 August 2024. Downloaded by Institute of Physics, CAS on 10/29/2024 4:28:02 AM.

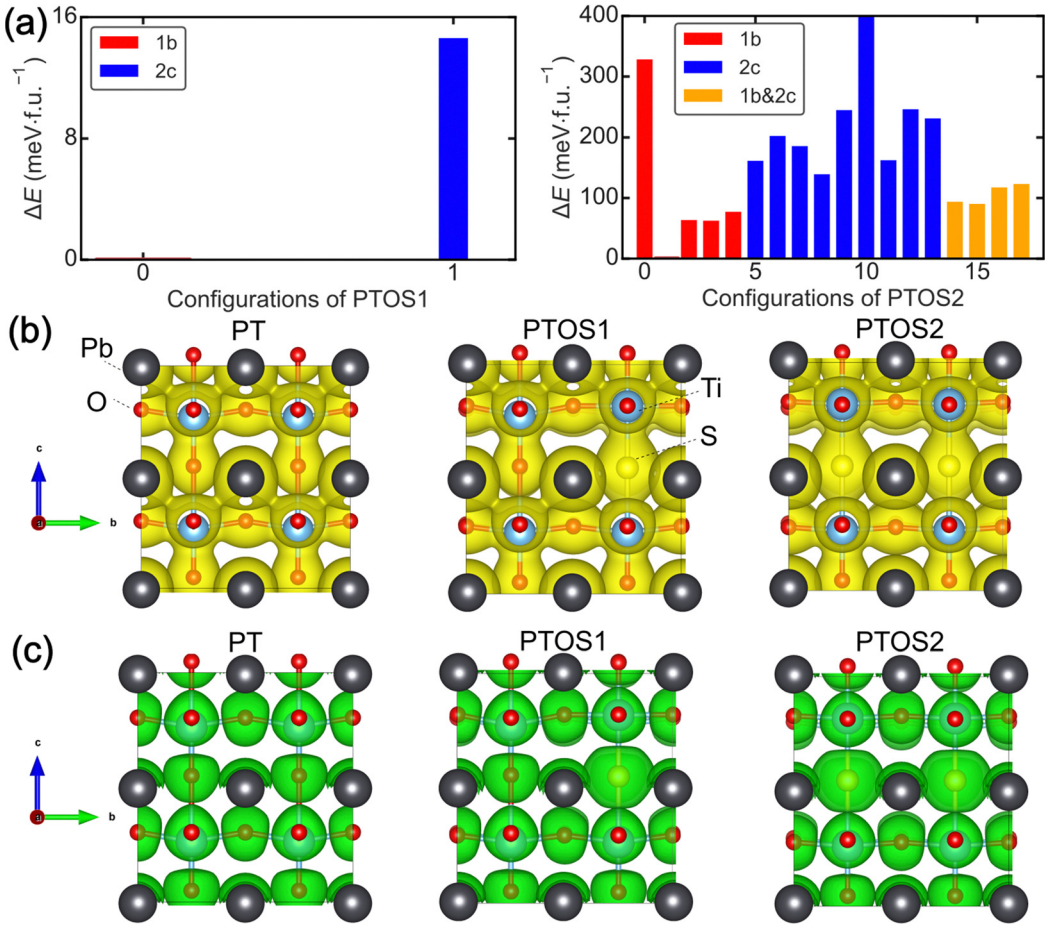

Fig. 4 Structural and electronic properties from DFT. (a) Energetic profiles for PTOS1 and PTOS2. The horizontal index indicates the 'ID' of the doped configurations in our calculations. The lowest energy configuration is chosen as the reference and is set to zero. (b) Charge density maps of PT, PTOS1 and PTOS2. (c) Electron localization functions of PT, PTOS1 and PTOS2, in which the isosurface is set to 0.5.

should be satisfied for the mechanical stability of a tetragonal system: $C_{11} > 0$, $C_{33} > 0$, $C_{44} > 0$, $C_{66} > 0$, $(C_{11} - C_{12}) > 0$, $(C_{11} + C_{33} - 2C_{13}) > 0$, $\{2(C_{11} + C_{12}) + C_{33} + 4C_{13}\} > 0$. We find all the elastic constants of PT, PTOS1 and PTOS2 are positive and satisfy the above conditions. This indicates that all the cases are mechanically stable. Taking the 40-atom PT supercell as an example, the values of C_{11}, C_{12}, C_{13}, C_{33}, C_{44}, and C_{66} are predicted to be 244 GPa, 97.9 GPa, 67.8 GPa, 53.5 GPa, 56.3 GPa and 99.8 GPa, respectively. Correspondingly, we show the phonon dispersions of the PT supercell in Fig. S5 (ESI†) and found the supercell structure is dynamically stable. Fig. 4(b) shows the comparison of the charge density maps of PT, PTOS1 and PTOS2. Upon doping, the hybridization between in-plane Ti and O atoms is slightly affected; in contrast, the overlap of the large volume of the isosurface of S and its neighboring out-of-plane Ti indicates the hybridization between S and Ti is strong along the [001] axis. By replacing O with S, we find the hybridization of the 1b anion site and the neighboring Pb is also enhanced. The above phenomena can be attributed to the fact that sulfur is more delocalized than oxygen. This delocalization can be understood because oxygen is more electronegative than sulfur and has a stronger tendency to attract electrons towards their nuclei. In Fig. 4(c), we also show the electron localization functions at an isosurface of 0.5. This also implies that the sulfur doping introduced more delocalized electronic states, which enhances the hybridization of Ti and S, as well as the hybridization between the dopants and the neighboring Pb. The evolution of the hybridization observed in the DFT calculations may be responsible for the enhanced NTE in the sulfur doped $PbTiO_3$.

The issue of achieving large NTE is vital; however, it remains challenging. The discovery of NTE materials provides a promising possibility because NTE materials can be used to compensate for general PTE by forming composites with NTE materials. Therefore, materials with controllable CTE can be developed, which is very important for practical applications. As the two key factors for the application of NTE materials, the magnitude of the NTE and the NTE operation window are critical. However, most currently available NTE materials show small magnitudes of NTE, and NTE occurs only in a narrow temperature range. The present work provides a new and effective route for exploring an enhanced NTE over a wide temperature range in PT-based ferroelectrics by introducing anion substitution at the O site. Under these guidelines, we also prepared other new mixed-anion PT-based compounds. A novel thermal expansion

 This journal is © The Royal Society of Chemistry 2024

Published on 13 August 2024. Downloaded by Institute of Physics, CAS on 10/29/2024 4:28:02 AM.

property is also expected. Thus, the introduction of anions is likely to be an effective method for controlling thermal expansion in currently known NTE materials with flexible structures. It is noted that the machine learning interatomic potentials (*e.g.* moment tensor potentials, MTP[51–53]) being developed in the latest years have enabled a relatively cheap way to studying the thermal properties at the macroscopic scale. The simulation of the oxysulfide of $PbTiO_3$ with machine learning interatomic potentials is interesting and will implement our understanding of the enhanced negative thermal expansion.

3. Conclusion

In summary, we successfully prepared the oxysulfide of $PbTiO_3$ using a high-pressure and high-temperature method to study the effect of anion substitution on the thermal expansion properties. We discovered that the tetragonality of pristine PT could be increased even with a small amount of S substitution for O. As a result, an enhanced NTE with an average volumetric CTE of $\bar{\alpha}_V = -2.50 \times 10^{-5}$ K^{-1} was achieved over a wide temperature range from RT up to 790 K, which is much stronger than that of pristine PT. Furthermore, first-principles calculations indicate that the enhanced tetragonality in the present PTOS system is attributed to the enhanced hybridization between Pb and O/S by the substitution of S. This work demonstrates a new technique for controlling the CTE of PT-based ferroelectric NTE materials, which can also be applied to other NTE materials with flexible structures.

4. Experimental section

Sample preparation

A series of $PbTiO_{3-x}S_x$ (x = 0–0.02, hereafter abbreviated as PTOS100x) compounds were prepared by the high-pressure and high-temperature (HPHT) method. The high-purity raw materials of PbO, PbS, and TiO_2 were thoroughly mixed according to the stoichiometric ratio. The mixtures were then sealed in a platinum capsule with a diameter of 3.6 mm and a height of 5.0 mm, followed by the HPHT treatment at 8 GPa and 1200 °C for 60 min using a cubic anvil-type apparatus.

Crystal structure analysis

The crystal structures of all the samples were characterized by means of laboratory X-ray powder diffraction (XRD) performed on a Brucker D8 ADVANCE diffractometer. Temperature-dependent synchrotron X-ray diffraction (SXRD) data were collected at the BL02B2 beamline of SPring-8 with a light wavelength of 0.42 Å.[54] The detailed structure analysis was performed with the same initial model as that of $PbTiO_3$ (space group: *P4mm*, no. 99) by the Rietveld method using the FullProf software.[55] The microstructural and elemental results were acquired on transmission electron microscopes (TEMs) (ARM200F with a field-emission gun (FEG) and JEM-2100 Plus) operating at 200 kV. Raman scattering spectra were collected on a MonoVista CRS+ 500 spectrometer (Spectroscopy & Imaging, Germany). X-ray absorption near edge spectroscopy (XANES) at the S-K edge was performed at beamline 4B7A of Beijing Synchrotron Radiation Facility (BSRF) *via* the fluorescence (FY) mode. The S and PbS^{2-} were also measured as S^0 and S^{2-} references, respectively. The self-consistent full multiple scattering calculation is performed using FDMNES (Joly 2009) software on a cluster with a radius of 6 Å.[56]

Electronic structure calculation

The structural and electronic properties of lead titanate and sulfur doped lead titanate were studied by density functional theory (DFT) methods implemented in the Vienna *ab initio* simulation package (VASP).[57,58] The GGA-type PBE exchange functional[59] was used with a cutoff energy of 500 eV. All the doped and pristine lead titanate models were simulated using a 2 × 2 × 2 40-atom supercell. PTOS1 and PTOS2 were approximately simulated by substituting one and two sulfur atoms in the supercells, respectively. The cell parameters of PT, PTOS1, and PTOS2 from the experiment were employed in the DFT calculations and fixed throughout the calculations accordingly. The coordinates, starting from the experimental data, were fully relaxed in calculations to ensure that the energy criterion of 10^{-6} eV and the force criterion of 0.005 eV per angstrom were satisfied. We also examined the spin–orbit coupling and found its effect on the electronic structure was negligible (see Fig. S6, ESI†). We also confirm that the major results of electronic structures are independent of the exchange functional (Fig. S7, ESI†).

Author contributions

Z. P. conceived the project. Z. P. synthesized the samples. Z. P., X. W., X. B. Y., L. F., Y. Y. W., and C. Y. M. performed the XANES measurements. Y.-W. F., Z. L., X. J., and Z. L. performed the theoretical calculations. Z. P., T.N., Y. S., Q. L., and S. K. performed the synchrotron X-ray diffraction experiments. X. S. and R. Y. measured and analyzed the TEM data. Z. P. wrote the manuscript. All authors discussed the results and commented on the manuscript. Z. P., M. A., X. R. X., and Y. L. guided the projects.

Data availability

All data needed to evaluate the conclusions in the paper are presented in the paper and/or the ESI.†

Conflicts of interest

The authors declare that they have no competing interests.

Acknowledgements

This work was supported by the National Key R&D Program of China (Grant No. 2021YFA1400300), the National Natural Science Foundation of China (22271309, 12304268, 11934017, 11921004, and 12261131499), the Grants-in-Aid for Scientific Research (JP18H05208 and JP19H05625) from the Japan Society for the Promotion of Science (JSPS), the Beijing Natural Science Foundation (Grant No. Z200007), the Chinese Academy of

Published on 13 August 2024. Downloaded by Institute of Physics, CAS on 10/29/2024 4:28:02 AM.

Sciences (Grant No. XDB33000000), and the Kanagawa Institute of Industrial Science and Technology. The synchrotron X-ray powder diffraction experiments were performed at SPring-8 with the approval of the Japan Synchrotron Radiation Research Institute (2023B1575 and 2024A1506). XANES at the S-K edge was performed at beamline 4B7A of Beijing Synchrotron Radiation Facility (BSRF). Technical and human support provided by the DIPC Supercomputing Center is gratefully acknowledged.

References

1 K. Takenaka, *Sci. Technol. Adv. Mater.*, 2012, **13**, 013001.
2 P. J. Attfield, *Front. Chem.*, 2018, **6**, 371.
3 J. Chen, L. Hu, J. X. Deng and X. R. Xing, *Chem. Soc. Rev.*, 2015, **44**, 3522–3567.
4 C. Linda, *Materials*, 2012, **5**, 1125–1154.
5 Q. Li, K. Lin, Z. Liu, L. Hu, Y. Cao, J. Chen and X. R. Xing, *Chem. Rev.*, 2022, **122**, 8438–8486.
6 T. A. Mary, J. S. O. Evans, T. Vogt and A. W. Sleight, *Science*, 1996, **272**, 90–92.
7 X. R. Xing, J. Deng, J. Chen and G. Liu, *Rare Metal*, 2003, **22**, 294–297.
8 X. X. Jiang, M. S. Molokeev, L. Dong, Z. Dong, N. Wang, L. Kang, X. Li, Y. Li, C. Tian, S. Peng, W. Li and Z. Lin, *Nat. Commun.*, 2020, **11**, 5593.
9 Y. W. Long, N. Hayashi, T. Saito, M. Azuma, S. Muranaka and Y. Shimakawa, *Nature*, 2009, **458**, 60–63.
10 M. Azuma, W. T. Chen, H. Seki, M. Czapski, S. Olga, K. Oka, M. Mizumaki, T. Watanuki, N. Ishimatsu, N. Kawamura, S. Ishiwata, M. G. Trucker, Y. Shimakawa and P. J. Attfield, *Nat. Commun.*, 2011, **2**, 347.
11 I. Yamada, K. Tsuchida, K. Ohgushi, N. Hayashi, J. Kim, N. Tsuji, R. Takahashi, M. Matsushita, N. Nishiyama, T. Inoue, T. Irifune, K. Kato, M. Takata and M. Takano, *Angew. Chem., Int. Ed.*, 2011, **50**, 6579–6582.
12 H. Yamamoto, T. Imai, Y. Sakai and M. Azuma, *Angew. Chem., Int. Ed.*, 2018, **57**, 8170–8173.
13 M. Sato, V. Warne-Lang, Y. Kadowaki, N. Katayama, Y. Okamoto and K. Takenaka, *AIP Adv.*, 2020, **10**, 075207.
14 N. Shi, A. Sanson, Q. Gao, Q. Sun, Y. Ren, Q. Huang, D. O. de Souza, X. R. Xing and J. Chen, *J. Am. Chem. Soc.*, 2020, **142**, 3088–3093.
15 M. V. Schilfgaarde, I. A. Abrikosov and B. Johansson, *Nature*, 1999, **400**, 46–49.
16 R. J. Huang, Y. Liu, W. Fan, J. Tan, F. Xiao, L. Tian and L. F. Li, *J. Am. Chem. Soc.*, 2013, **135**, 11469–11472.
17 Y. Song, J. Chen, X. Liu, C. Wang, J. Zhang, H. Liu, H. Zhu, L. Hu, K. Lin, S. Zhang and X. R. Xing, *J. Am. Chem. Soc.*, 2018, **140**, 602–605.
18 Y.-Y. Zhao, F.-X. Hu, L.-F. Bao, J. Wang, H. Wu, Q.-Z. Huang, R.-R. Wu, Y. Liu, F.-R. Shen, H. Kuang, M. Zhang, W.-L. Zuo, X.-Q. Zheng, J.-R. Sun and B.-G. Shen, *J. Am. Chem. Soc.*, 2015, **137**, 1746–1749.
19 K. Lin, W. Li, C. Yu, S. Jiang, Y. Cao, Q. Li, J. Chen, M. Zhang, M. Xia, Y. Chen, K. An, X. Li, Q. Zhang, L. Gu and X. R. Xing, *Acta Mater.*, 2020, **198**, 271–280.
20 J. Lin, P. Tong, K. Zhang, H. Tong, X. Guo, C. Yang, Y. Wu, M. Wang, S. Lin, L. Chen, W. Song and Y. Sun, *Appl. Phys. Lett.*, 2016, **109**, 241903.
21 K. Takenaka and H. Takagi, *Appl. Phys. Lett.*, 2005, **87**, 261902.
22 X. Y. Song, Z. Sun, Q. Z. Huang, M. Rettenmayr, X. Liu, M. Seyring, G. Li, G. Rao and F. Yin, *Adv. Mater.*, 2011, **23**, 4690.
23 C. Wang, L. Chu, Q. Yao, Y. Sun, M. Wu, L. Ding, J. Yan, Y. Na, W. Tang, G. Li, Q. Huang and J. W. Lynn, *Phys. Rev. B: Condens. Matter Mater. Phys.*, 2012, **85**, 220103(R).
24 B. K. Greve, K. L. Martin, P. L. Lee, P. J. Chupas, K. W. Chapman and A. Wilkinson, *J. Am. Chem. Soc.*, 2010, **132**, 15496–15498.
25 L. Hu, J. Chen, L. Fan, Y. Ren, Y. Rong, Z. Pan, J. Deng, R. Yu and X. R. Xing, *J. Am. Chem. Soc.*, 2014, **136**, 13566–13569.
26 J. Chen, Q. Gao, A. Sanson, X. Jiang, Q. Huang, A. Carnera, C. G. Rodriguez, L. Olivi, L. Wang, L. Hu, K. Lin, Y. Ren, Z. Lin, C. Wang, L. Gu, J. Deng, J. P. Attfield and X. R. Xing, *Nat. Commun.*, 2017, **8**, 14441.
27 F. Qin, J. Chen, U. Aydemir, A. Sanson, L. Wang, Z. Pan, J. Xu, C. Sun, Y. Ren, J. Deng, R. Yu, L. Hu, G. J. Snyder and X. R. Xing, *Inorg. Chem.*, 2017, **56**, 10840–10843.
28 D. Wendt, E. Bozin, J. Neuefeind, K. Page, W. Ku, L. Wang, B. Fultz, A. V. Tkachenko and I. A. Zaliznyak, *Sci. Adv.*, 2019, **5**, eaay2748.
29 A. L. Goodwin, M. Calleja, M. J. Conterio, M. T. Dove, J. S. O. Evans, D. A. Keen, L. Peters and M. G. Tucker, *Science*, 2008, **319**, 794–797.
30 Q. Gao, J. Chen, Q. Sun, D. Chang, Q. Huang, H. Wu, A. Sanson, R. Milazzo, H. Zhu, Q. Li, Z. Liu, J. Deng and X. R. Xing, *Angew. Chem., Int. Ed.*, 2017, **129**, 9151–9156.
31 Q. Gao, J. Wang, A. Sanson, Q. Sun, E. Liang, X. R. Xing and J. Chen, *J. Am. Chem. Soc.*, 2020, **142**, 6935–6939.
32 T. F. Qi, O. B. Korneta, S. Parkin, L. E. De Long, P. Schlottmann and G. Cao, *Phys. Rev. Lett.*, 2010, **105**, 177203.
33 K. Takenaka, Y. Okamato, T. Shinoda, N. Katayama and Y. Sakai, *Nat. Commun.*, 2017, **8**, 14102.
34 L. Hu, Y. Zhu, Y.-W. Fang, M. Fukuda, T. Nishikubo, Z. Pan, Y. Sakai, S. Kawaguchi, H. Das, A. Machida, T. Watanuki, S. Mori, K. Takenaka and M. Azuma, *Chem. Mater.*, 2021, **33**, 7665–7674.
35 S. C. Abrahams, S. K. Kurtz and P. B. Jamieson, *Phys. Rev.*, 1968, **172**, 551–553.
36 J. Chen, X. Xing, R. Yu and G. Liu, *J. Am. Ceram. Soc.*, 2005, **88**, 1356–1358.
37 J. Chen, X. Xing, R. Yu and G. Liu, *Appl. Phys. Lett.*, 2005, **87**, 231915.
38 T. Yang, Y. Wang, L. Fan, N. Wang, K. Lin, J. Chen and X. R. Xing, *J. Phys. Chem. C*, 2020, **124**, 20445–20449.
39 J. Chen, X. Xing, G. Liu, J. Li and Y. Liu, *Appl. Phys. Lett.*, 2006, **89**, 101914.
40 Z. Pan, J. Chen, R. Yu, L. Patra, P. Ravindran, A. Sanson, R. Milazzo, A. Carnera, L. Hu, L. Wang, H. Yamamoto, Y. Ren, Q. Huang, Y. Sakai, T. Nishikubo, T. Ogata, X. A. Fan, Y. Li, G. Li, H. Hojo, M. Azuma and X. R. Xing, *Chem. Mater.*, 2019, **31**, 1296–1303.

 This journal is © The Royal Society of Chemistry 2024

Published on 13 August 2024. Downloaded by Institute of Physics, CAS on 10/29/2024 4:28:02 AM.

41 E. K. Dempsey and J. Cumby, *Chem. Commun.*, 2024, **60**, 2548–2551.
42 M. Croft, W. Caliebe, H. Woo, T. A. Tyson, D. Sills, Y. S. Hor, S.-W. Cheong, V. Kiryukhin and S.-J. Oh, *Phys. Rev. B: Condens. Matter Mater. Phys.*, 2003, **67**, 201102.
43 S. Y. Kuo, C. T. Li and W. F. Hsieh, *Appl. Phys. Lett.*, 2002, **81**, 3019–3021.
44 Z. Pan, J. Chen, X. Jiang, L. Hu, R. Yu, H. Yamamoto, T. Ogata, Y. Hattori, F. Guo, X. A. Fan, Y. Li, G. Li, H. Gu, Y. Ren, Z. Lin, M. Azuma and X. R. Xing, *J. Am. Chem. Soc.*, 2017, **139**, 14865–14868.
45 F. Wang, Y. Xie, J. Chen, H. Fu and X. R. Xing, *Appl. Phys. Lett.*, 2013, **103**, 221901.
46 J. Chen, F. Wang, Q. Huang, L. Hu, X. Song, J. Deng, R. Yu and X. R. Xing, *Sci. Rep.*, 2013, **3**, 2458.
47 R. E. Cohen, *Nature*, 1992, **358**, 136–138.
48 Y. Kuroiwa, S. Aoyagi, A. Sawada, J. Harada, E. Nishibori, M. Takata and M. Sakata, *Phys. Rev. Lett.*, 2001, **87**, 217601.
49 F. Mouhat and F.-X. Coudert, *Phys. Rev. B: Condens. Matter Mater. Phys.*, 2014, **90**, 224104.
50 D. C. Wallace, *Thermodynamics of Crystal*, Wiley, 1972.
51 B. Mortazavi, E. V. Podryabinkin, I. S. Novikov, T. Rabczuk, X. Y. Zhuang and A. V. Shapeev, *Comput. Phys. Commun.*, 2021, **258**, 107583.
52 A. V. Shapeev, *Multiscale Model. Simul.*, 2016, **14**, 1153–1173.
53 B. Mortazavi, E. V. Podryabinkin, S. Roche, T. Rabczuk, X. Y. Zhuang and A. V. Shapeev, *Mater. Horiz.*, 2020, **7**, 2359–2367.
54 S. Kawaguchi, M. Takemoto, K. Osaka, E. Nishibori, C. Moriyoshi, Y. Kubota, Y. Kuroiwa and K. Sugimoto, *Rev. Sci. Instrum.*, 2017, **88**, 085111.
55 G. Shirane, R. Pepinsky and B. C. Frazer, *Acta Crystallogr.*, 1956, **9**, 131–140.
56 O. Bunău and Y. Joly, *J. Phys.: Condens. Matter*, 2009, **21**, 345501.
57 G. Kresse and J. Furthmüller, *Phys. Rev. B: Condens. Matter Mater. Phys.*, 1996, **54**, 11169–11186.
58 G. Kresse and J. Furthmüller, *Comput. Mater. Sci.*, 1996, **6**, 15–50.
59 J. P. Perdew, K. Burke and M. Ernzerhof, *Phys. Rev. Lett.*, 1996, **77**, 3865–3868.